行政院國家科學委員會補助專題研究計畫成果報告

****
* 新型光電材料、元件及雷射光源(II)－ *
* 子計畫三：半導體光放大器內非線性現象之數值研究(II) *
****

計畫類別：整合型計畫

計畫編號：NSC 89-2215-E-002-033

執行期間：八十八年八月一日至八十九年七月三十一日

計畫主持人：江衍偉，國立台灣大學電信工程學研究所

執行單位：國立台灣大學電信工程學研究所

中華民國八十九年十月二十日

行政院國家科學委員會專題研究計畫成果報告

新型光電材料、元件及雷射光源(II)—
子計畫三：半導體光放大器內非線性現象之數值研究(II)
Numerical Study on Nonlinear Phenomena in Semiconductor Optical Amplifiers (II)

計畫編號：NSC 89-2215-E-002-033
執行期限：八十八年八月一日至八十九年七月三十一日
主持人：江衍偉，國立台灣大學電信工程學研究所
計畫參與人員：周卓平、陳鴻祥、王志洋、陳祖傑，國立台灣大學電信工程學研究所

摘要

吾人分析了一全半導體光放大器非線性光環元件之脈波操作特性。數值模擬包括自我開關與雙脈波之交互開關等。
關鍵詞：光學開關，半導體光放大器

Abstract

Efficient pulsed-signal operation of an all-semiconductor-optical-amplifier nonlinear optical loop device is numerically demonstrated. The simulations include the self-switching and pump-probe configurations.
Keywords: optical switches, semiconductor optical amplifiers

All-optical switching devices based on nonlinear Sagnac interferometry are attractive for high-speed communications and signal processing. Usually, such a device includes a loop structure for providing power-dependent gain/phase modulation and a 2x2 coupler for signal splitting/combination. Therefore, the loop structure needs to contain some material to produce certain nonlinear optics mechanism. When the signal passes through the coupler and splits into the loop, the two counter-propagating components experience different gain/phase modulations. This difference determines the distribution of signal power between two output ports of the coupler. Because the difference in gain/phase modulation depends on the input power level, the output power of the device can be controlled by the input power, resulting in switching effect.

This kind of device was first implemented as a nonlinear optical loop mirror (NOLM), consisting of a fiber loop and a fiber coupler [1]. However, to enhance the optical nonlinearity and to reduce the size of device, semiconductor optical amplifiers (SOA) are incorporated or even used to replace the fibers in the device. Recently, we have reported the fabrication and continuous wave (cw)-signal operation of an all-SOA nonlinear loop device [2,3]. The configuration of this device is the same as an NOLM, including an SOA loop and a multimode-interference waveguide amplifier (MMIWA) for closing the loop. With cw signals, efficient all-optical switching was observed.

In this report, we investigate the pulsed-signal operation of a similar device. Here the asymmetric loop structure plays a crucial role. The power-dependent switching results from the combined effects of asymmetric gain/phase modulation in the loop and nonlinear coupling in the MMIWA. To demonstrate all-optical switching function, the pump-probe configuration is also numerically simulated.

Figure 1 shows the layout of our nonlinear loop device. The device consists of several parts: the loop, the MMIWA, the input port and the output port. Note that the one-quarter and three-quarter sections of the

loop are now divided for different injection currents (I_4 and I_3, respectively). The injection currents for the regions of MMIWA and input/output portion are I_2 and I_1, respectively. Good passivation was made for disconnecting the four injection areas. All parts are made of ridge-loading waveguide SOA's. The loop with a ridge width of 4 μm (expected to form a single-lateral-mode waveguide) is connected to the MMIWA with a ridge of 8 μm wide where two modes can propagate. The input and output ports also have a ridge width of 4 μm. By injecting different currents, we can control the gain factors in different parts of the device. In experiment, the all-SOA nonlinear loop device is fabricated with a GaAs/AlGaAs four-period multiple quantum well epitaxial structure [2].

In device operation, counter-propagating light waves exist simultaneously in the SOA. To simulate the colliding pulses in the MMIWA, we expand the TE-polarized electric field into two waveguide modes, each of which propagates in both forward and backward directions. In the loop region, only counter-propagating single-mode fields exist. In either the MMIWA or loop, we solve a set of differential equations for the forward- and backward-propagating wave fields as well as the rate equation for the carrier density. For simplicity, we have ignored any gain or loss in the input/output legs of the device. For numerical computation, the time-domain traveling-wave method [4] is employed to treat the counter-propagation problem. However, instead of using the first-order finite-difference approximation to the partial derivatives, we analytically solve the differential equations in each division segment along the waveguide axis to increase the numerical accuracy. The parameter values include the operating wavelength at 0.84 μm, the FWHM pulse width at 2 psec, the coupling length of the MMIWA at 526 μm, the linewidth enhancement factor at 12, the carrier lifetime at 1 nsec, the internal loss coefficient of the MMIWA (loop) at $1000m^{-1}$ ($2000\ m^{-1}$), and the effective waveguide area at 8 μm x 0.43 μm (4 μm x 0.43 μm) for the MMIWA (loop).

In the following simulations, the length of the loop is fixed at 1.895 mm and the length of the MMIWA is 250 μm. The small-signal gain factors of the one-quarter loop, the three-quarter loop, and the MMIWA are set to be 35 dB, 5 dB, and 2 dB, respectively. Figure 2 shows the power-dependent self-switching result, describing the output pulse energy versus the input pulse energy. The thick solid curve, the dashed curve, and the thin solid curve represent the output pulse energy emerging from the output port, from the input port, and the sum of the two, respectively. In interpreting the device operation with cw signals, we considered the nonlinear coupling effect in the MMIWA and the functions of the lateral field redistribution and amplification from the loop [3]. Such considerations are still valid for pulsed signals. However, with the pulsed signals the loop asymmetry needs to be taken into account. The nonlinear coupling in the MMIWA results in power-dependent lateral field distribution. After splitting into the two counter-propagating components in the loop, they experience different gain levels and phase shifts in the asymmetric loop. Such differences then combine with the nonlinear coupling effect during the backward propagation in the MMIWA to give further distribution of the signal power between the input and output ports.

To investigate the cross-switching phenomena, we conduct the pump-probe simulation. Figures 3 and 4 show the output energy of the probe pulse (from the output port, from the input port, or the sum from both ports) as a function of pump-probe time delay, where the positive time delay means that the pump signal leads the probe signal. Here, the input energy of the pump pulse is 0.015 pJ and that of the probe pulse is 0.002 pJ. Again, both the pump and probe are of pulse width 2 psec. When the probe leads the pump sufficiently, corresponding to a large negative time delay in Fig. 3, the probe signal is not affected by the pump as expected. This corresponds to the linear

optics case, and little energy comes out from the output port. As the probe leads the pump by a small time interval, say, several psec, the counterclockwise propagating probe pulse in the loop will collide with the clockwise propagating pump pulse in the high-gain one-quarter loop region. On the other hand, the clockwise propagating probe pulse in the loop collides with the counterclockwise propagating pump pulse in the low-gain three-quarter loop region. The strong asymmetric gain/phase modulation experienced by the counter-propagating probe signal gives rise to the severe variation of the probe energy with respect to the time delay. This explains the occurrence of the peak of the probe energy from the output port. When the pump leads the probe by a small time interval, corresponding to a small positive time delay in Fig. 3, the gain in SOA is saturated just in advance by the pump pulse. Therefore, less gain/phase modulation can be experienced by the probe, resulting in less variation of the probe energy. As the pump leads the probe even further, the probe pulse just sees the already saturated and gradually recovered environment. No significant asymmetric nonlinearity is now experienced by the probe, corresponding to the linear optics case. From Fig. 4, it is seen that the output probe energy gradually attains its unsaturated level with the time delay of the order of nanoseconds. This is consistent with the fact that the carrier lifetime here is assumed to be 1 nsec.

In summary, the pulsed-signal operation of an all-semiconductor-optical-amplifier loop device has been numerically demonstrated, showing efficient power-dependent self-switching and cross-switching effects. It is found that the asymmetric gain distribution along the loop is crucial for efficient pulsed-signal operation.

References

1. N. J. Doran and D. Wood, "Nonlinear-optical loop mirror," Opt. Lett., Vol. 13, pp. 56-58, 1988.
2. J. H. Lee, D. A. Wang, H. J. Chiang, D. W. Huang, S. Gurtler, C. C. Yang, Y. W. Kiang, B. C. Chen, M. C. Shih and T. J. Chuang, "Nonlinear switching in an all-semiconductor-optical-amplifier loop device," IEEE Photon. Technol. Lett., Vol. 11, pp. 236-238, 1999.
3. J. H. Lee, D. A. Wang, Y. W. Kiang, H. J. Chiang and C. C. Yang, "Nonlinear switching behaviors in a compact all-semiconductor optical-amplifier Sagnac interferometer device," IEEE J. Quantum Electron., Vol. 35, pp. 1469-1477, 1999.
4. L. M. Zhang, S. F. Yu, M. C. Nowel, D. D. Marcenac, J. E. Carroll, and R. G. S. Plumb, "Dynamic analysis of radiation and side-mode suppression in a second-order DFB laser using time-domain large-signal traveling wave model," IEEE J. Quantum Electron., Vol. 30, pp. 1389-1395, 1994.

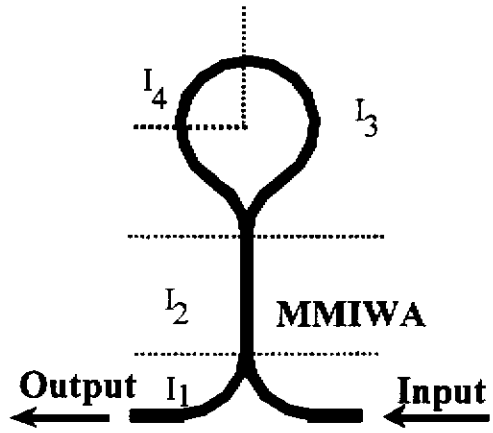

Fig. 1 Layout of the all-semiconductor nonlinear loop device.

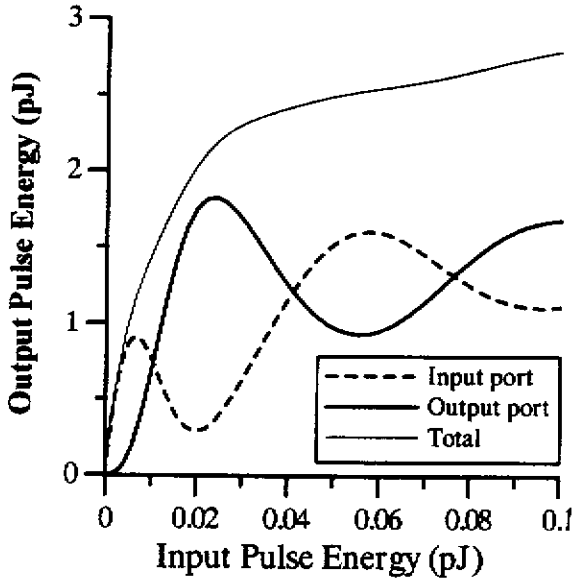

Fig. 2 Output pulse energy (from output port, from input port, or the sum from both ports) versus input pulse energy.

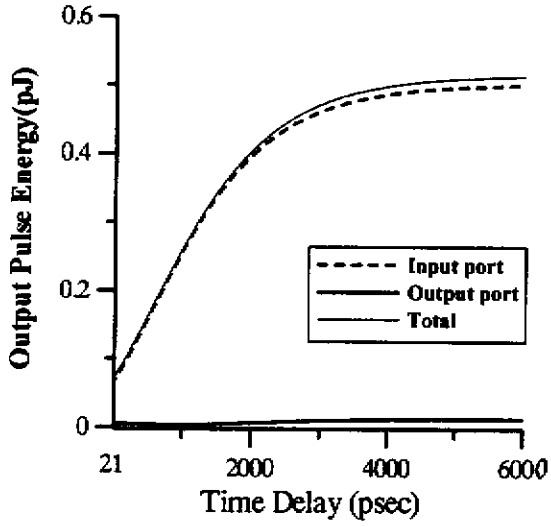

Fig. 4 Output energy of the probe signal (from output port, input port, or the sum from both ports) as a function of time delay between the pump and probe.

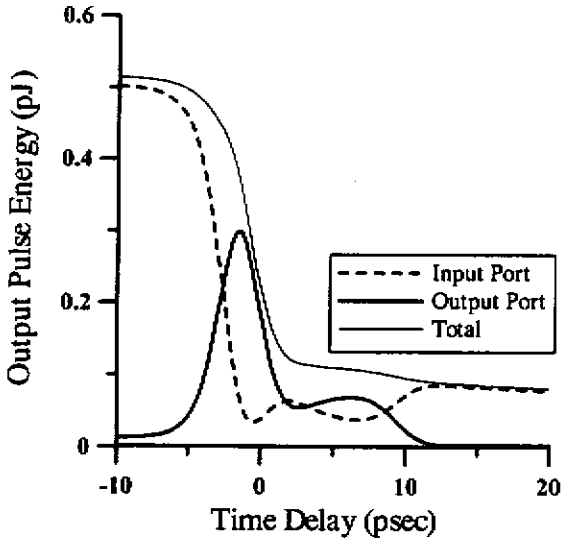

Fig. 3 Output energy of the probe signal (from output port, input port, or the sum from both ports) as a function of time delay between the pump and probe.